2018 IEEE/RSJ International Conference on Intelligent Robots and Systems (IROS)
Madrid, Spain, October 1-5, 2018

# 3D-printed flexure-based finger joints for anthropomorphic hands*

L. Garcia, M. Naves and D.M. Brouwer
Precision Engineering
Faculty of Engineering Technology
University of Twente
7500 AE Enschede, The Netherlands
d.m.brouwer@utwente.nl

***Abstract*— Flexure-based finger joints for prosthetic hands have been studied, but until now they lack stiffness and load bearing capacity. In this paper we present a design which combines large range of motion, stiffness and load bearing capacity, with an overload protection mechanism. Several planar and non-planar hinge topologies are studied to determine load capacity over the range of motion. Optimized topologies are compared, in 30 degrees deflected state, in terms of stresses by deflection and grasping forces. Additionally, support stiffnesses were computed for all hinges in the whole range of motion (45 degrees). The Hole Cross Hinge presented the best performance over the range of motion with a grasping force up to 15 N while deflected 30 degrees. A new concept, the Angle Three-Flexure Cross Hinge, provides outstanding performance for deflections from 17.5 up to 30 degrees with a 20 N maximum grasping force when fully deflected. Experimental verification of the support stiffness over the range of motion shows some additional compliances, but the stiffness trend of the printed hinge is in line with the model. The presented joints power grasping capability outperform current state flexure-base hands and are comparable to commercial non-flexure-based prosthetic hands. In the event of excessive loads, an overload protection mechanism is in place to protect the flexure-hinges.**

***Index Terms*— Compliant joints, flexures, robotic hand, prosthetic hand, anthropomorphic, additive manufacturing.**

## NOMENCLATURE

| | |
|---|---|
| MCP | Metacarpophalangeal. |
| ROM | Range of motion. |
| E | Young's modulus. |
| G | Shear modulus. |
| SLS | Selective laser sintering |

## I. INTRODUCTION

Flexure joints applied in prosthetic and robotic hands have been of interest in recent years [1]–[4]. Some of the advantages of an integrated flexure design are more stable grasps and a reduced number of parts [3]–[5]. Furthermore, when 3D-printing technology is used to manufacture a prosthetic hand as a single monolithic structure, absence of assembly can be achieved reducing overall costs.

A major challenge for flexure joints in large range of motion applications is the strong decrease of support stiffness in load carying directions when deflected [6]–[8]. This loss of support stiffness for large range of motions led to reconsideration of flexures in the MCP joint and the accompanying poor load carrying capacity currently prevents widespread applicability in robotic and prosthetic hands [3]. Therefore, it is of interest to study the mechanical behavior of monolithic integrated flexure joint designs over the whole range of motion. The decrement of the stiffness in the support direction also leads to loss of load bearing capacity of the hand. Especially when including tendon actuation and high grasping forces, elastic instability of the joint (buckling) can result in reduced load-carrying capacity.

Researchers from the UB Hand compared several flexure topologies for robotic hands by analyzing compliance matrices in undeflected position [4], [9]. Additionally, Tavakoli et al. presented new topologies and analyzed the flexure stresses and deflections for the undeflected state [1]. Although analyzing the stiffness properties of flexure topologies at undeflected state allows the use of simple linear beam equations, it gives no lead to the stiffness properties at larger deflection angles due to the strong non-linear behavior. Furthermore, as critical stiffness and load typically occurs at maximum deflection angle, stiffness at maximum deflection angle is of primary interest rather than at the undeflected state.

Kalpathy used a pseudo-rigid-body model with an approximation of Timoshenko beam theory to model leafsprings in a larger range of motion [2]. Although pseudo rigid-body modeling allows for larger deflections, it is limited to simulation of its kinematic behavior and stiffness in the free motion direction. Therefore, evaluation of the support stiffness at large deflection angles is still unavailable.

Odhner presented the "Smooth Curvature model" to calculate compliance matrices in large deflections of planar leafspring designs, as this can be associated with stable grasps [10]. This method allows for evaluation of support stiffness at larger deflections, however, it described the compliance matrix only for the 2-dimensional case. For typical loading-conditions, out-of-plane stiffness and load carrying capacity are important also. Furthermore, it only allows for the evaluation of planar hinge designs.

In this paper, we exploit a flexible multibody method to calculate and optimize several flexure hinge topologies, including non-planar topologies, during a cylindrical medium

*This work was supported by the program of Science Based Engineering of the Engineering Technology Faculty of the University of Twente

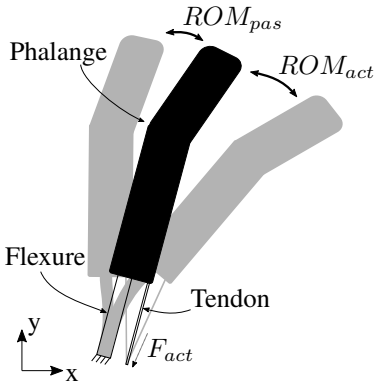


Fig. 1. Passive and active range of motion.

power wrap (Fig. 2). This power grasp is identified as one of the most common used grasps [11], [12] and therefore the main focus of this research. First, we developed an optimization strategy to minimize stresses and maximize grasping force for each topology in deflected state. Secondly, several joints are presented and the optimized topologies are compared. The comparison is based on stresses due to grasping force and sideways loads. Furthermore, a comparison of the support stiffnesses over the whole range of motion for the different topologies is done. Third, an overload protection mechanism for the sideways force is presented. An FEM analysis is used to obtain the stiffness of the entire finger, which is subsequently corroborated with measurements. This methodology results in the first flexure-based finger joint with substantial external load capacity and grasping force evaluated in the full-ROM.

## II. DESIGN METHODOLOGY

### A. Optimization loadcase

To enable flexures in the MCP joint we have carefully balanced the range of motion with the load capacity and the torsional stiffness requirements. A finger is designed to be in a rest position that allows $15°$ of passive extension ($ROM_{pas}$) and $-30°$ of active flexion ($ROM_{act}$), Fig. 1. This range of motion allows to grasp majority of objects in the medium wrap range [13].

Since the fingers have high compliance for rotations around the z-axis, the passive extension is achieved by contact with an object. The contact will open the hand to allow bigger objects to be grasped if so required. The compliance of the joint is generally insufficient to grip objects.

The extension is actuated by a tendon force $F_{act}$ which deflects the flexure up to $-30°$ around the z-axis.

The MCP has been identified as the critical joint [3]. When holding an object the contact force and weight of an object result in a combination of in- and out-of-plane bending loads of the flexure elements, Fig. 2.

Since it is of interest to study the functionality of hands while power grasping, a contact point common to all hinge topologies is defined (Fig. 2). By doing so, there is a similar effect of the loads on the hinges and the shape of the finger is independent of the size of the hinge.

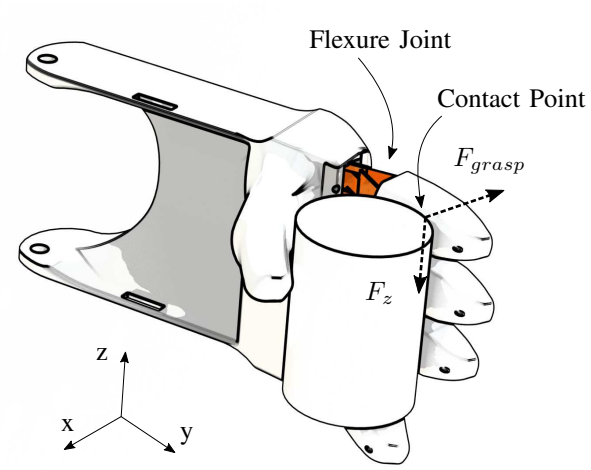


Fig. 2. Reaction forces during power grasping.

For the optimization, the tendon is actuated to position the finger at $-30°$ of rotation. In the same plane a normal contact force, $F_{grasp} = 5$ N, is applied in the contact point. While the contact force $F_{grasp}$ attempts to open the hand, the actuation force $F_{act}$ in the tendon is increased such to maintain contact. Additionally, a $F_z = 0.5$ N sideways force in the z-direction plane is loaded in the contact point.

### B. Workspace

The workspace is defined based on anthropomorphic dimensions of a human hand [14]. For the proximal joint (MCP) a workspace is used allowing for 60 x 18 x 17 mm, corresponding to the length, width and thickness respectively. Width and thickness represent an average of the proximal joint dimensions of all fingers, both for male and female, except the thumb.

The length of the hinge is designed so that half of it is inside of the palm, see Fig. 2. By doing so, the center of rotation of the flexure hinge is at the end of the palm and beginning of the finger, equivalent to the location in a human hand. The proximal phalange acts as a housing for the other half of the joint.

### C. Hinge Topologies

A series of hinge topologies are defined in advance, see Fig. 4, and their performance during power grasp is compared.

- Leafspring (LS)
- Solid-Flexure Cross Hinge (SFCH)
- Three-Flexure Cross Hinge (TFCH)
- Hole Cross Hinge (HCH)
- Angled Three-Flexure Cross Hinge (ATFCH)

The initial topologies are designed such that in the undeflected position there is one rotational degree of freedom, for flexion and extension of the fingers, and the stiffnesses in support directions are high. For comparison, a flexure hinge consisting of only a single leafspring is evaluated too, which only provides support stiffnesses in three degrees of freedom. This topology is used as a reference as it is often used for prosthetic and robotic hands [2]–[4]. An initially

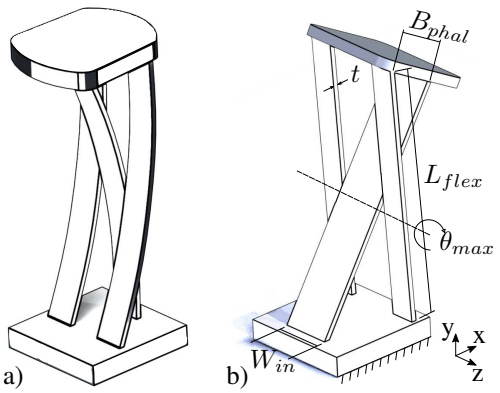


Fig. 3. Angled Three-Flexure Cross Hinge with design parameters ($L_{flex}$, $B_{phal}$, $W_{in}$ and $t$). a) Undeflected position with pre-curved flexures; b) deflected position with straightened flexures.

curved design is added to generate high support stiffness at large deflections while sacrificing stiffness at smaller deflections. Several of these hinges were defined previously by [7] including their design parameters $\mathbf{p}$.

The HCH combines the constant bending moment of a TFCH, with the full width of SFCH, except at the crossing where reinforced parts are used.

The concept of the ATFCH is introduced in this paper, with a similar topology to the TFCH. The hinge is defined such to obtain straight elements when a specific angle is achieved, Fig. 3b.

The length of the leafsprings are equal, as the diagonals of an isosceles trapezoid, to have an even stress distribution during deflection around the z-axis. This hinge is parametrized by the parameter vector $\mathbf{p}$.

$$\mathbf{p} = \begin{Bmatrix} L_{flex} & B_{phal} & W_{in} & t \end{Bmatrix} \tag{1}$$

Where $L_{flex}$ is the length of elements, $B_{phal}$ is the distance of the base (short side of the isosceles trapezoid), $W_{in}$ is the width of the inner element and $t$ is the thickness of the elements, see Fig. 3.

### D. Optimization

Flexible multibody software SPACAR is used to evaluate the performance of the intrinsic geometric nonlinearities of the hinges [15]. By using nonlinear 3D beam elements, it is possible to efficiently compute the performance of a series of design parameters in large displacement motions and small elastic deformations. As a result a relatively small number of elements produce accurate results at low computational cost.

A shape optimization based on the Nelder Mead method is used. The objective is to find the set of design parameters $\mathbf{p}$ that maximize the performance within the specified constraints [16].

The method minimizes a cost function $\mathcal{F}(\mathbf{p})$ which is defined to achieve the lowest ratio between stress and grasping force at $-30°$ of flexion.

$$\mathcal{F}(\mathbf{p}) = \lambda \frac{\sigma(\mathbf{p})}{F_{grasp}} \tag{2}$$

Where $\lambda$ is a performance "penalty" (soft constraint) to unfeasible solutions [16], $F_{grasp}$ is the grasping force and $\sigma(\mathbf{p})$ is the stress value defined as follows,

$$\sigma(\mathbf{p}) = \begin{cases} \sigma_{limit} & \text{if} \quad \max \sigma(\mathbf{p}) \geq \sigma_{limit} \\ \max \sigma(\mathbf{p}) & \text{if} \quad \max \sigma(\mathbf{p}) < \sigma_{limit} \end{cases} \tag{3}$$

$$F_{grasp} = \begin{cases} F_{grasp} \text{ @ } \sigma_{limit} & \text{if} \quad \max \sigma(\mathbf{p}) \geq \sigma_{limit} \\ \max F_{grasp} & \text{if} \quad \max \sigma(\mathbf{p}) < \sigma_{limit} \end{cases} \tag{4}$$

$$\lambda = \max_{\theta} \left( \frac{d_z(\mathbf{p}, \theta) - d_{z.max}}{d_{z.max}} \right) \tag{5}$$

The stress $\sigma_{limit}$ is defined as $60\%$ of the maximum allowable stress of the material, $\sigma_{max}$. The objective to introduce this stress limit is to filter out flexure hinges that show high stresses by only deflection. These hinges would result in low capacity for carrying grasping loads.

The "penalty" factor shown in 5 corresponds to the deflections in z-direction $d_z$ due to sideways force $F_z$. Where $d_z(\mathbf{p}, \theta)$ is the deflection for the current set of parameters $\mathbf{p}$ and $d_{z.max}$ is the maximum allowable deflection. A similar performance "penalty" is also applied for the allowable stress $\sigma_{max}$ (Table I) of the material and dimensions exceeding the defined workspace. An additional penalty is applied when flexures collide to ensure collision free designs [17]. By applying these penalties on the cost function, soft constraints are added to the unconstrained Nelder Mead algorithm [16].

For each iteration in the Nelder Mead algorithm $N + 1$ cost functions ($N$ equal to the number of design parameters) are compared and sorted according to $\mathcal{F}(\mathbf{p_1}) \leq \mathcal{F}(\mathbf{p_2}) \leq \ldots \leq \mathcal{F}(\mathbf{p_{N+1}})$, being $\mathcal{F}(\mathbf{p_1})$ the solution with lowest cost (highest performance). Based on these results, a new parameter set $\mathbf{p}$ is determined and added to the set of solutions. This process continues until a certain convergence criteria is satisfied, defined by:

$$\frac{\mathcal{F}(\mathbf{p_1})}{\mathcal{F}(\mathbf{p_{N+1}})} > 0.995 \tag{6}$$

which corresponds to $0.5\%$ deviation in performance in the current set of solutions [16].

Eight shape optimizations per hinge topology were conducted, each one with a different initial parameter set. In each optimization a global or local optimum can be obtained. By conducting several optimizations the probability of finding a solution within $5\%$ of the global optimum is greatly increased. For example, when conducting eight optimizations for the Three-Flexure Cross Hinge the probability of finding a solution within $5\%$ of the global optimum is approximately $97\%$ [16].

### E. Experimental Setup

In order to validate the numerical model, a setup for measuring stiffness is used, Fig. 5. A parallel guidance, 1-DOF in the gravity direction, is actuated when weights are added to the end effector. The vertical displacement is

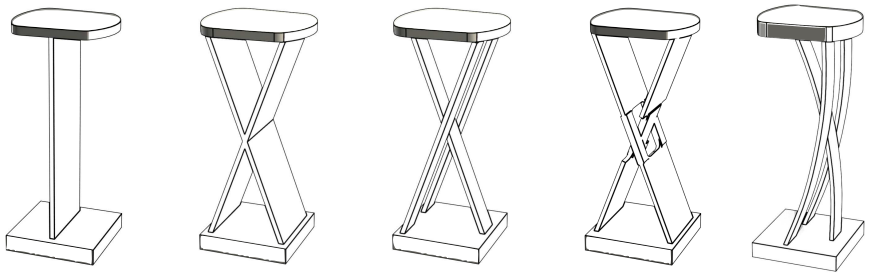


Fig. 4. Hinge Topologies in undeflected state. (a) Leafspring, LS; (b) Solid-Flexure Cross Hinge, SFCH; (c) Three-Flexure Cross Hinge, TFCH; (d) Hole Cross Hinge, HCH; (e) Angled Three-Flexure Cross Hinge, ATFCH.

measured through a linear variable differential transformer (LVDT) sensor. The strain energy storage of the parallel guidance has been take into account.

The finger is clamped at one end with all DOFs constrained. At the free end, two translations are constrained by wire flexures. The first wire flexure attaches the parallel guidance to the free end, which simulates the force $F_z$ from Fig. 2. The second wire flexure maintains the finger at the desired deflection (0°, -15° and -30°).

A finger with only the MCP joint was printed in nylon PA12 using an SLS process [18]. SLS allows full spatial design freedom without the necessity of support structures, and it allows high quality printing of nylon types with better strain properties than ABS and PLA for example, which is important for flexures.

In the finger the section corresponding to the median phalange is hollow with a shell of 1.5 mm, the distal phalange is printed with a 100% infill.

## III. RESULTS

A series of optimized hinges were found by evaluating the cost function $\mathcal{F}(\mathbf{p})$ at a contact force $F_{grasp} = 5$ N and sideways force $F_z = 0.5$ N while a deflection of $-30°$ was maintained.

After the optimizations were completed a sideways load $F_z = 2$ N and an increasing grasping force on the contact point was modeled at a deflection of $\theta_{max} = -30°$, Fig. 6. This allowed the understanding of failure mechanisms of the optimized hinges.

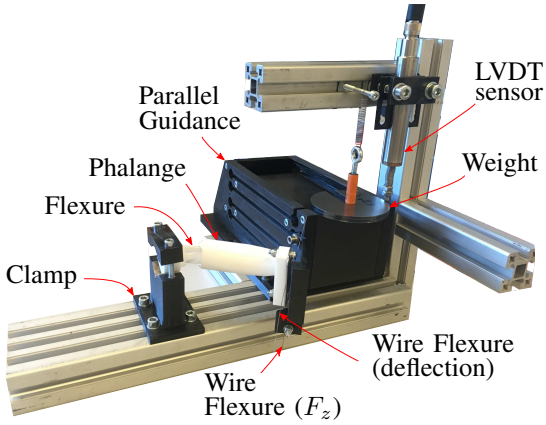


Fig. 5. Experimental setup for stiffness measurement.

TABLE I

OPTIMIZATION PARAMETERS [18]

| Parameter | Unit | |
|---|---|---|
| $\theta_{min}/\theta_{max}$ | | $-15°/30°$ |
| $t_{min}/t_{max}$ | mm | 0.5/2.5 |
| E | GPa | 1.7 |
| $\sigma_{limit}$ | MPa | 35.0 |
| $\sigma_{max}$ | MPa | 50.0 |
| $\sigma_{max}$ / E | | $29.4 \cdot 10^{-3}$ |

When an object is going to be grasped, first a tendon force $F_{act}$, required to close the hand, is increased. This produces stress ($\sigma_{flex}$) in the flexure hinge. When the object is grasped and held, a combination of grasping force, increased tendon force and the sideways loads generate further stresses on the hinge.

The initial stress shown in Fig. 6 is only caused by deflection of the hinges, $\sigma_{flex}$. The ratio between the maximum allowable stress of the material ($\sigma_{max}$ in Table I) and the stress due to deflection, $\sigma_{max}/\sigma_{flex}$, is lower than 2.5 for the Leafspring, the Hole Cross Hinge and Three-Flexure Cross Hinge. On the other extreme, the Solid-Flexure Cross Hinge accounts for a ratio lower than 1.6. In general, a higher ratio is desired for flexure mechanisms that are going to be cyclically loaded.

From $F_{grasp} > 1$ N the object is being grasped and held in the air. At this point the initial stress $\sigma_{flex}$ adds with the induced stress by the constant sideways force, the grasping force and the tendon force required to keep the finger in place. A steep increase of the stresses is observed for the

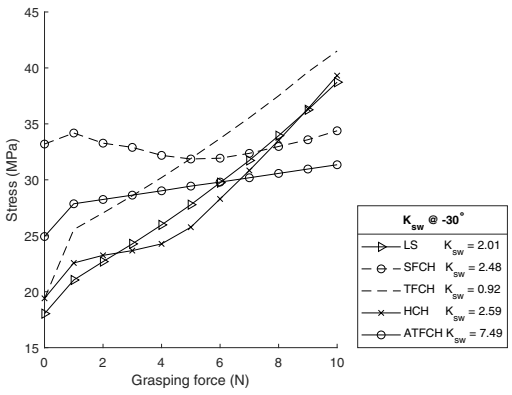


Fig. 6. Comparison of optimized hinge topologies deflected at $-30°$, with sideways force $F_z = 2$ N.

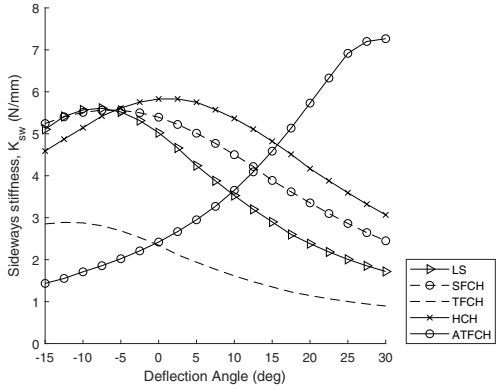


Fig. 7. Comparison of optimized hinge topologies over the range of motion while loaded with a sideways force $F_z = 2$ N.

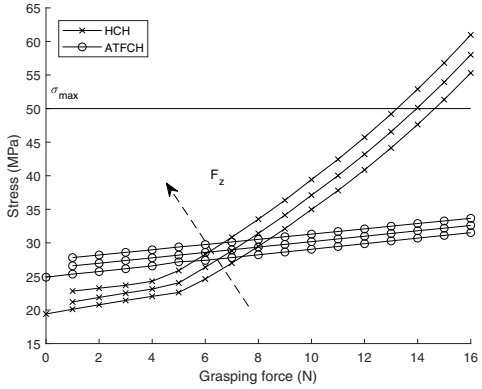


Fig. 8. Influence of sideways force ($F_z = [0; 1; 2]$ N) in optimized Angled Three-Flexure Cross Hinge (ATFCH) and Hole Cross Hinge (HCH).

hinges with the lowest $\sigma_{max}/\sigma_{flex}$ ratio.

The Angled Three-Flexure Cross Hinge is a balance between a ratio $\sigma_{max}/\sigma_{flex} = 2$ and a low slope stress/contact force.

The Solid-Flexure Cross Hinge presents elastic instability, at 11 N of contact force, due to high tendon forces. Although it shows a steady stress behavior because it is stiffer in all directions compared to the other flexures.

The sideways stiffness $K_{sw}$ presented in Fig. 6 is the inverse ratio between a measured displacement $d_z$ at the contact point and the applied load $F_z = 2$ N at $-30°$. $K_{sw}$ is affected by both translational compliance in z, and rotational compliances with the rotation axis in the x/y plane.

$$K_{sw} = \frac{F_z}{d_z} \tag{7}$$

The Three-Flexure Cross Hinge displayed the lowest $K_{sw}$ stiffness while the Angled Three-Flexure Cross Hinge presented the best performance as expected, due to the straight flexures at the deflected position.

Further analysis of $K_{sw}$, Fig. 7, in the range of motion was studied. In this case a tendon force was applied to deflect the flexure joint to an specific angle. At that moment a load $F_z = 2$ N was applied and a $K_{sw}$ was calculated as described in 7.

The Hole Cross Hinge has the best performance over the range of motion, with a drop of support stiffness of $47.4\%$. The Angled three-flexurec cross hinge outperformed for deflection angles above $17.5°$, but over the whole range of motion shows a drop of stiffness of $80\%$. The Leafspring, the Three-Flexure Cross Hinge and the Solid-Flexure Cross Hinge show differences above $50\%$ in the support stiffness from undeflected to deflected position.

From Fig. 7 a non-symmetry between extension and flexion can be observed. In extension, the flexures are deflected but the influence of the torsion component is diminished. This is due to an alignment of the contact point with the center of rotation along the y-axis.

The Hole Cross Hinge and the Angled Three-Flexure Cross Hinge have resulted in hinge topologies with better performance. To compare the hinges in more detail, they were submitted to a deflection of $-30°$ and load $F_{grasp}$ and $F_z$ are increased up to the maximum load carrying capacity to gain insight in failure behavior of the hinges.

Fig. 8 shows that the stress for the Hole Cross Hinge surpasses the allowable stress limit $\sigma_{max}$ at $F_{grasp} = 15$ N. The change of the stress behavior presented at $F_{grasp} = 5$ N is due to increasing tendon $F_{act}$ in an already deflected hinge.

The Angled Three-Flexure Cross Hinge presented a linear and steady increase of the stresses until $F_{grasp} = 21$ N, where elastic instability appears.

Odhner reported grasping forces as high as $21.5$ N for a three finger robotic hand with flexure hinges only in the proximal joint position [3]. The latter measurement was accomplished in a grasping position that avoided sideways forces. While Belter reported holding forces at the tip for commercial non-flexure-based prosthetic hands in a range between $3 - 16$ N [19]. The presented performance of the Hole Cross Hinge and the Angled Three-Flexure Cross Hinge are a considerable improvement to current flexure-based hands and can be compared to current commercial non-flexure-based prosthetic hands [19].

### A. Experimental test

Before measuring the finger, the parallel guidance was characterized and the stiffness was measured when loaded up to displacements of $4.3$ mm. The stiffness of the parallel guidance was linear in the whole range of motion. This was used later in order to subtract from the stiffness of the finger, as these are in parallel.

With the experimental setup, shown in Fig. 5, $\begin{bmatrix}0° & -15° & -30°\end{bmatrix}$ deflections angles were tested for a Hole Cross Hinge. These measurements are compared for validation with the flexible multibody and FEM model in Fig. 9.

Differences of $60\%$ were found between the flexible multibody analysis and the experimental results. This model considers the attachment of the finger and the phalange as rigid. By comparison the FEM included the phalange as a deformable body. At $0°$ the difference can be attributed to the clamp of the finger. As the deflection increases the loss of stiffness of the hinge becomes more important than the clamping. For this reason the differences between the FEM

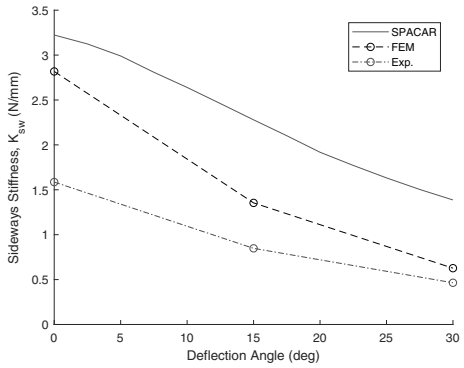


Fig. 9. Comparison of sideways stiffness obtained by experimental test, flexible multibody analysis and FEM.

and the experimental at $-30°$ are $25\%$. Small compliances in any element contribute significantly as these elements are in series. Despite the differences, the efficiency of the flexible multibody analysis over the FEM makes it attractive for efficient flexure hinge optimizations.

### B. Overload Protection Mechanism

A mechanism that prevents failure of the flexures when loads are over the limits is proposed. The concept prevents excessive displacements in torsion and in mostly all support directions with the exception of loading in positive y-direction. An initial kinematic analysis resulted in the geometry shown in Fig. 10.

In Fig. 10b contact is produced by excessive torsion on the finger. Also, when overloading due to lateral (x-direction) or compression forces (negative y-direction), a rolling contact is still possible between the palm and the phalange.

## IV. CONCLUSIONS

In this paper five flexure-based finger joints topologies are presented, optimized and compared. The joints were kept within stress limits of 50 MPa and MCP joint human dimensions while a combination of $45°$ large range of motion, grasping force of 20 N and sideways load of 2 N was carried out. The topologies have been designed to withstand relatively high tendon actuation forces. The Hole Cross Hinge showed the best combination of high grasping force and low stress over the range of motion. The Angled Three-Flexure Cross Hinge however performs particularly good near the end of the range of motion at full flexion, and has the highest grasping force capacity. Experimental verification of the support stiffness over the range of motion shows some additional compliances, but the stiffness trend of the printed hinge is in line with the model. The presented joints power grasping capability outperform current state of the art flexure-base hands and are comparable to commercial non-flexure-based prosthetic hands. In the event of excessive loads, an overload protection mechanism is in place to protect the flexure-hinges.

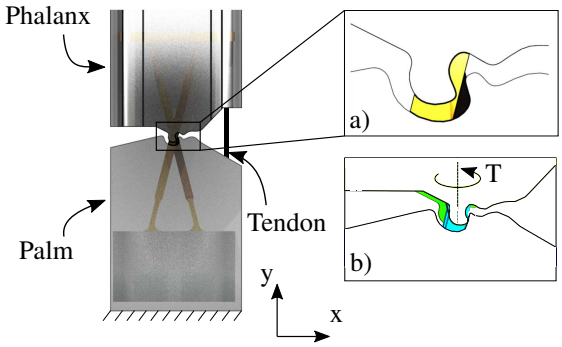


Fig. 10. Overload mechanism for a Hole Cross Hinge. a) Zoom at the center of rotation; b) Contact when excessive load is present.

## ACKNOWLEDGMENT

We thank W. Pot for his contribution to the experiments.

## REFERENCES

[1] M. Tavakoli, A. Sayuk, J. Lourenço, and P. Neto, "Anthropomorphic finger for grasping applications: 3D printed endoskeleton in a soft skin," *Int. J. Adv. Manuf. Technol.*, 2017.

[2] V. Kalpathy and H.-J. Su, "A 3-Spring Pseudo-Rigid-Body Model for Soft Joints with Significant Elongation Effects A 3-Spring Pseudo-Rigid-Body Model for Soft Joints with Significant Elongation Effects," *J. Mech. Robot.*, 2016.

[3] L. U. Odhner, L. P. Jentoft, M. R. Claffee, N. Corson, Y. Tenzer, R. R. Ma, M. Buehler, R. Kohout, R. D. Howe, and A. M. Dollar, "A compliant, underactuated hand for robust manipulation," *Int. J. Rob. Res.*, vol. 33, no. 5, pp. 736–752, 2014.

[4] G. Berselli, F. Parvari Rad, R. Vertechy, and V. Parenti Castelli, "Comparative evaluation of straight and curved beam flexures for selectively compliant mechanisms," *2013 IEEE/ASME Int. Conf. Adv. Intell. Mechatronics Mechatronics Hum. Wellbeing, AIM*, 2013.

[5] B. P. Trease, Y.-M. Moon, and S. Kota, "Design of Large-Displacement Compliant Joints," *J. Mech. Des.*, vol. 127, no. 4, p. 788, 2005.

[6] D. Brouwer, J. Meijaard, and J. B. Jonker, "Large deflection stiffness analysis of parallel prismatic leaf-spring flexures," *Precis. Eng.*, 2013.

[7] D. Wiersma, S. E. Boer, R. Aarts, and D. Brouwer, "Design and Performance Optimization of Large Stroke Spatial Flexures," *J. Comput. Nonlinear Dyn.*, vol. 9, no. January 2014, 2013.

[8] S. Awtar, "Analysis of Flexure Mechanisms in the Intermediate Displacement Range," in *Handb. Compliant Mech.*, L. L. Howell, S. P. Magleby, and B. M. Olsen, Eds. John Wiley & Sons Ltd, 2013.

[9] G. Berselli, A. Guerra, G. Vassura, and A. O. Andrisano, "An engineering method for comparing selectively compliant joints in robotic structures," *IEEE/ASME Trans. Mechatronics*, 2014.

[10] L. U. Odhner and A. M. Dollar, "The smooth curvature model: An efficient representation of Euler-Bernoulli flexures as robot joints," *IEEE Trans. Robot.*, vol. 28, no. 4, pp. 761–772, 2012.

[11] I. M. Bullock, J. Z. Zheng, S. De La Rosa, C. Guertler, and A. M. Dollar, "Grasp frequency and usage in daily household and machine shop tasks," *IEEE Trans. Haptics*, vol. 6, no. 3, pp. 296–308, 2013.

[12] C. Cipriani, M. Controzzi, and M. Carrozza, "The SmartHand transradial prosthesis," *J. Neuroeng. Rehabil.*, 2011.

[13] T. Feix, J. Romero, H.-b. Schmiedmayer, A. M. Dollar, and D. Kragic, "The GRASP Taxonomy of Human Grasp Types," *IEEE Transactions on Human-Machine Systems*, 2016.

[14] A. Freivalds, *Biomechanics of Upper Limbs: mechanics, modeling, and musculoskeletal injuries*. Boca Raton, Florida: CRC Press, 2004.

[15] J. B. Jonker and J. Meijaard, *SPACAR — Computer Program for Dynamic Analysis of Flexible Spatial Mechanisms and Manipulators*. Springer Berlin Heidelberg, 1990.

[16] M. Naves, D. Brouwer, and R. Aarts, "Building Block-Based Spatial Topology Synthesis Method for Large-Stroke Flexure Hinges," *J. Mech. Robot.*, vol. 9, no. 4, p. 041006, 2017.

[17] M. Naves, R. Aarts, and D. Brouwer, "Efficient collision detection method for flexure mechanisms comprising deflected leafsprings," *submited to ASME J. Mech. Robot.*

[18] EOS GmbH, "PA 2200 Performance 1.0." [Online]. Available: https://www.utwente.nl/en/rpl/Data%20sheets/Formiga%20P110/pa2200-preformance-1.0.pdf

[19] J. T. Belter, J. L. Segil, A. M. Dollar, and R. F. Weir, "Mechanical design and performance specifications of anthropomorphic prosthetic hands: a review." *J. Rehabil. Res. Dev.*, 2013.